Comparison of s-process abundances to meteorite data and the impact of neutron-capture cross sections on the Mo isotopic ratios

Maria Lugaro[1,2,3,4], **Mattias Ek[5*]**, Mária Pető[1,2], Marco Pignatari[1,2,6], Georgy V. Makhatadze[7], Isaac J. Onyett[7] and Maria Schönbächler[5]

[1] Konkoly Observatory, Research Centre for Astronomy and Earth Sciences, Eötvös Loránd Research Network (ELKH), Konkoly Thege M. út 15-17, 1121, Budapest, Hungary
[2] CSFK, MTA Centre of Excellence, Konkoly Thege Miklós út 15-17, 1121, Budapest, Hungary
[3] Institute of Physics, ELTE Eötvös Loránd University, Pázmány Péter sétány 1/A, 1117, Budapest, Hungary
[4] School of Physics and Astronomy, Monash University, 3800, Clayton, VIC, Australia
[5] Institute for Geochemistry and Petrology, ETH Zürich, Zurich, Switzerland
[6] E. A. Milne Centre for Astrophysics, University of Hull, Cottingham Road, HU6 7RX, Kingston upon Hull, UK
[7] Centre for Star and Planet Formation (StarPlan), Globe Institute, Faculty of Health and Medical Sciences, University of Copenhagen, Øster Voldgade 5-7, 1350, Copenhagen K, Denmark
*mattias.ek@erdw.ethz.ch

Eur. Phys. J. A (2023) 59:53
https://doi.org/10.1140/epja/s10050-023-00968-y

THE EUROPEAN PHYSICAL JOURNAL A

Regular Article - Theoretical Physics

Representation of *s*-process abundances for comparison to data from bulk meteorites

Maria Lugaro[1,2,3,4,a], Mattias Ek[5], Mária Pető[1,2], Marco Pignatari[1,2,6], Georgy V. Makhatadze[7], Isaac J. Onyett[7], Maria Schönbächler[5]

[1] Konkoly Observatory, Research Centre for Astronomy and Earth Sciences, Eötvös Loránd Research Network (ELKH), Konkoly Thege M. út 15-17, Budapest 1121, Hungary
[2] CSFK, MTA Centre of Excellence, Konkoly Thege Miklós út 15-17, Budapest 1121, Hungary
[3] Institute of Physics, ELTE Eötvös Loránd University, Pázmány Péter sétány 1/A, Budapest 1117, Hungary
[4] School of Physics and Astronomy, Monash University, Clayton, VIC 3800, Australia
[5] Institute for Geochemistry and Petrology, ETH Zürich, Zurich, Switzerland
[6] E. A. Milne Centre for Astrophysics, University of Hull, Cottingham Road, Kingston upon Hull, HU6 7RX, UK
[7] Centre for Star and Planet Formation (StarPlan), Globe Institute, Faculty of Health and Medical Sciences, University of Copenhagen, Øster Voldgade 5-7, 1350 Copenhagen K, Denmark

Translation of Stellar Yield Predictions for Comparison with the Laboratory Analysis of Meteorites

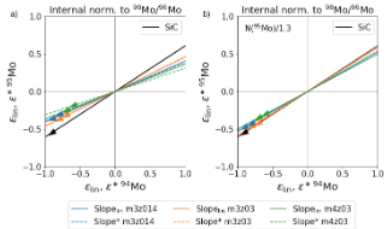

A git repository with a Jupyter notebook providing the tools to translate predictions from stellar yield calculations into the units and representation obtained from laboratory analysis of meteorites.

The repository is available on GitHub.

Cosmochemistry is the study of physical samples, most often meteorites or meteorite components.

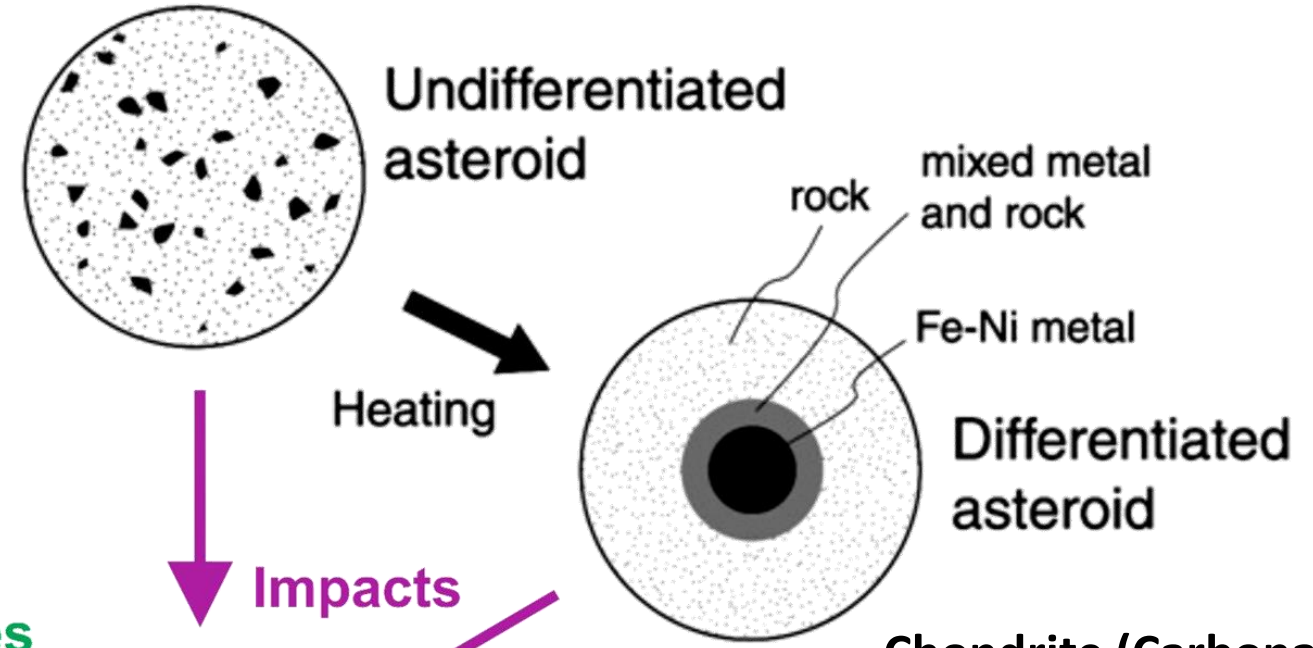

Iron Meteorite (IIAB)

Chondrite (Carbonaceous)

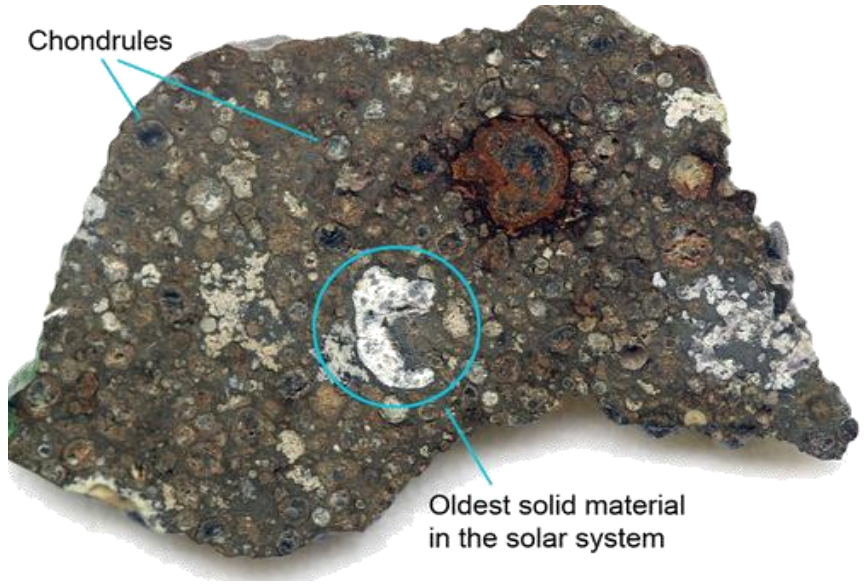

Isotopic varations in meteorites

Mass independent isotope variations can be generated by

- Heterogenous distribution of nucleosynthetic material
- Radioactive decay
- Exposure to galactic cosmic rays

Mass dependent isotope variations can arise from

- Geological/biological processes
- Chemical seperation of elements
- Isotopic analysis

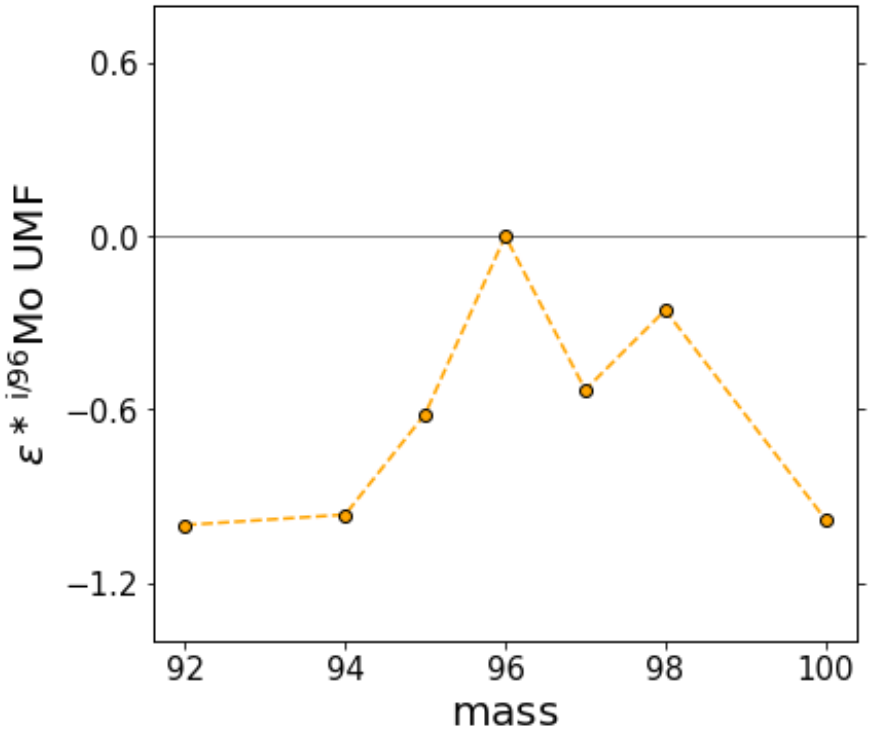

To remove the effects of mass dependent fractionation from an analysis we can **internally normalise** the sample.

$$\varepsilon R_{ij} = \left(\frac{R_{ij}^{SMP}}{R_{ij}^{STD}} - 1 \right) \times 10^4$$

Isotopic varations in meteorites

Mass independent isotope variations can be generated by

- Heterogenous distribution of nucleosynthetic material
- Radioactive decay
- Exposure to galactic cosmic rays

Mass dependent isotope variations can arise from

- Geological/biological processes
- Chemical seperation of elements
- Isotopic analysis

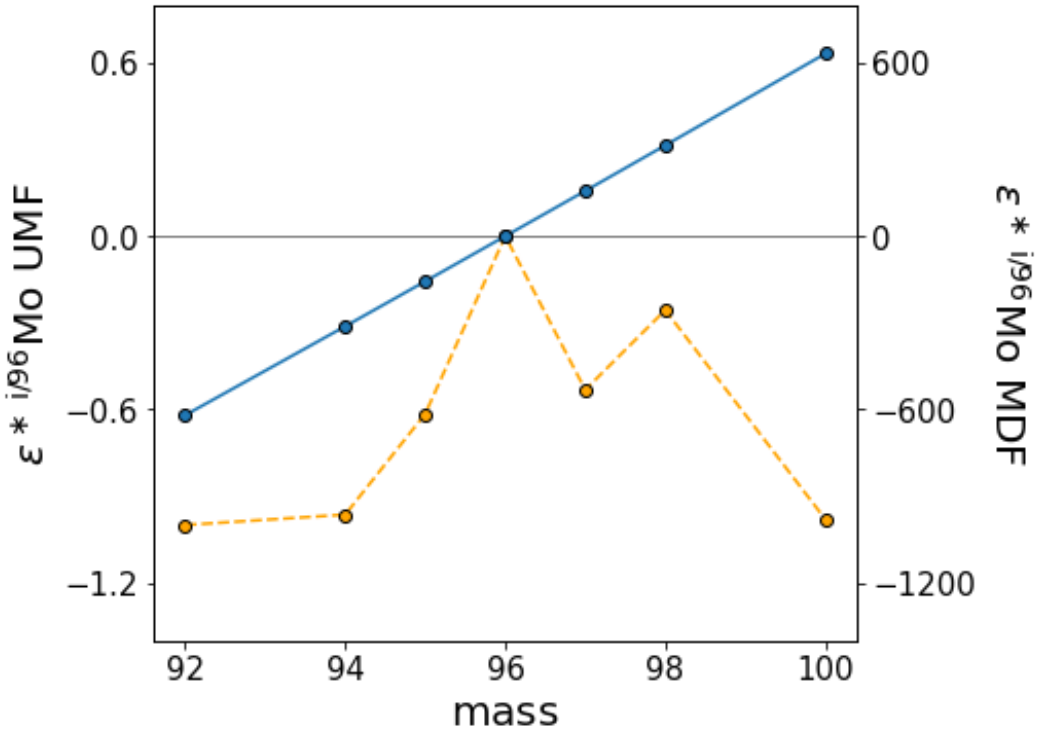

To remove the effects of mass dependent fractionation from an analysis we can **internally normalise** the sample.

$$\varepsilon R_{ij} = \left(\frac{R_{ij}^{SMP}}{R_{ij}^{STD}} - 1\right) \times 10^4$$

Instrumental mass fractionation follows the exponential law,

$$R_{ij} = r_{ij}\left(\frac{m_i}{m_j}\right)^{-\beta}$$

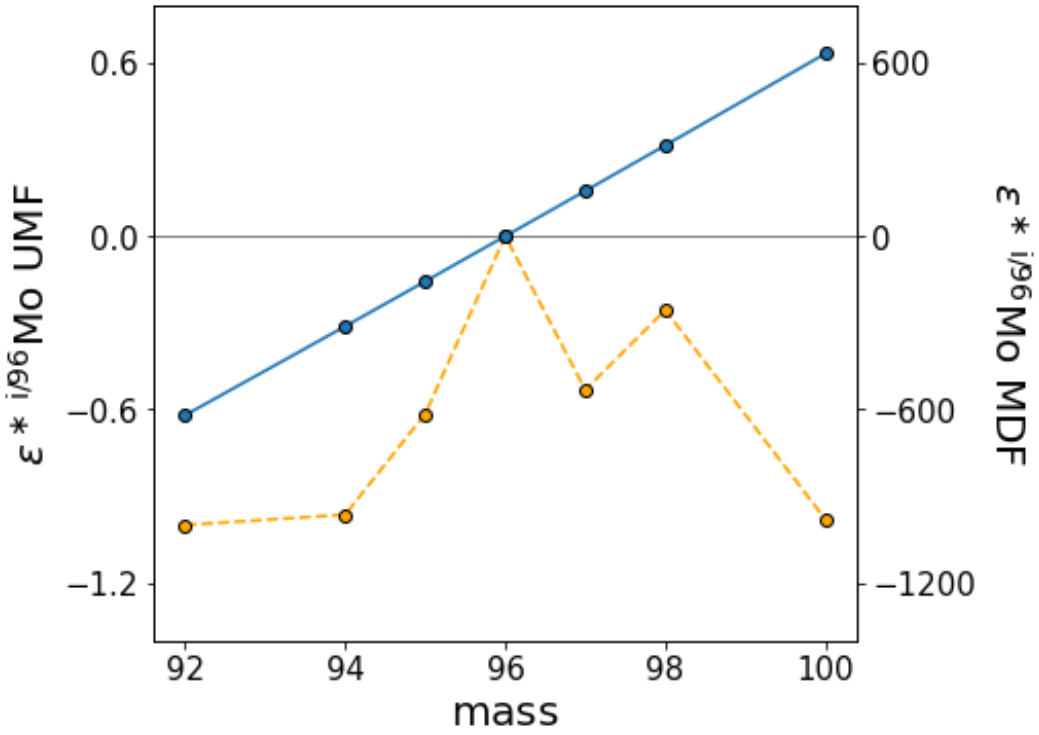

$$\varepsilon R_{ij} = \left(\frac{R_{ij}^{SMP}}{R_{ij}^{STD}} - 1\right) \times 10^4$$

Instrumental mass fractionation follows the exponential law,

$$R_{ij} = r_{ij}\left(\frac{m_i}{m_j}\right)^{-\beta}$$

Internal normalisation is correcting for mass fractionation by assuming a fixed value for a certain isotope ratio,

$$R_{ij} = r_{ij}\left(\frac{R_{kj}^{STD}}{r_{kj}^{SMP}}\right)^{\frac{\ln(m_i)-\ln(m_j)}{\ln(m_k)-\ln(m_j)}}$$

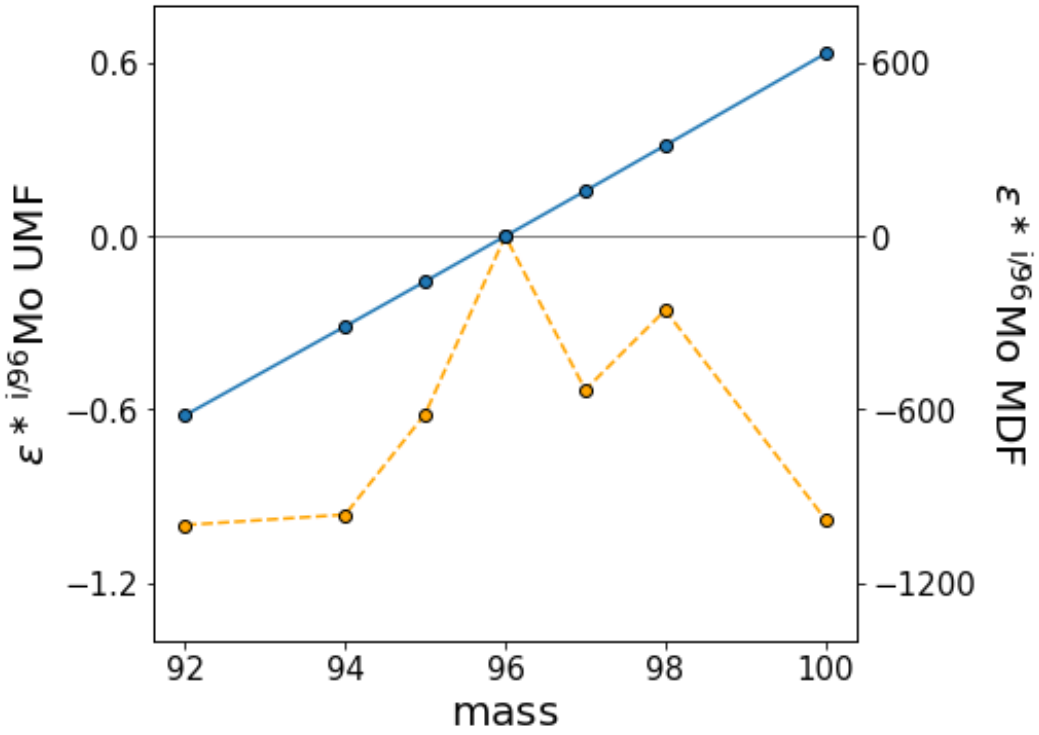

$$\varepsilon R_{ij} = \left(\frac{R_{ij}^{SMP}}{R_{ij}^{STD}} - 1\right) \times 10^4$$

Instrumental mass fractionation follows the exponential law,

$$R_{ij} = r_{ij}\left(\frac{m_i}{m_j}\right)^{-\beta}$$

Internal normalisation is correcting for mass fractionation by assuming a fixed value for a certain isotope ratio,

$$R_{ij} = r_{ij}\left(\frac{R_{kj}^{STD}}{r_{kj}^{SMP}}\right)^{\frac{\ln(m_i)-\ln(m_j)}{\ln(m_k)-\ln(m_j)}}$$

Including the epsilon notation we get the following,

$$\varepsilon R_{ij}^{SMP} = \left[\left(\frac{r_{ij}^{SMP}}{R_{ij}^{STD}}\right)\left(\frac{r_{kj}^{SMP}}{R_{kj}^{STD}}\right)^{-Q_i} - 1\right] \times 10^4$$

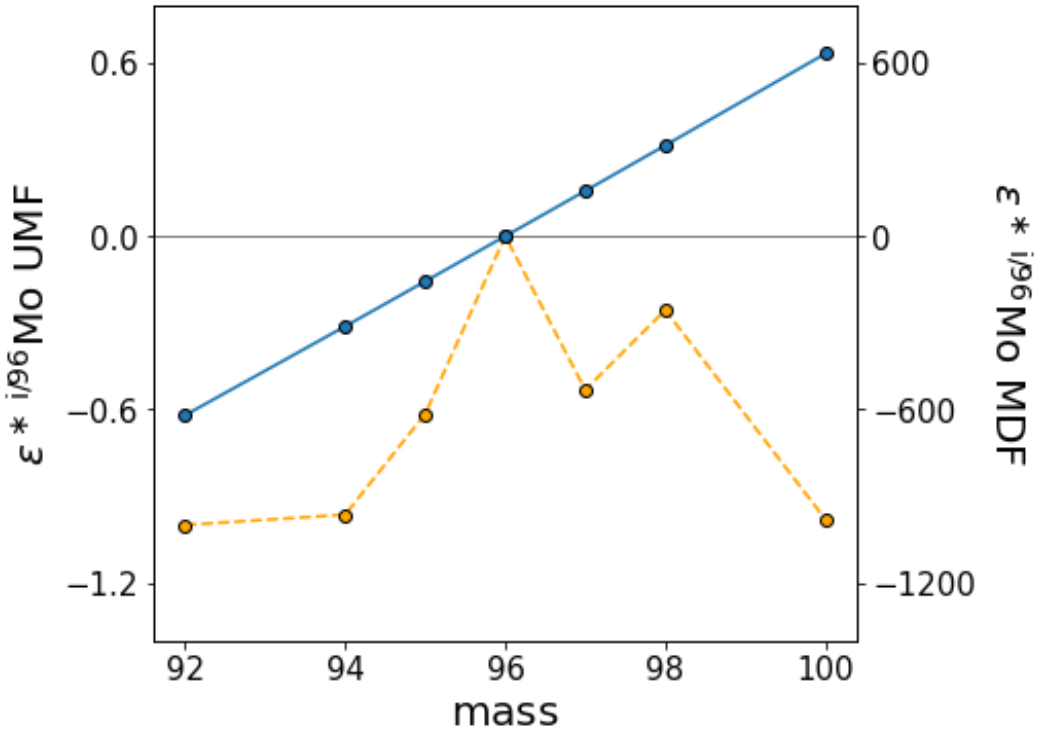

$$\varepsilon R_{ij} = \left(\frac{R_{ij}^{SMP}}{R_{ij}^{STD}} - 1\right) \times 10^4$$

Instrumental mass fractionation follows the exponential law,

$$R_{ij} = r_{ij}\left(\frac{m_i}{m_j}\right)^{-\beta}$$

Internal normalisation is correcting for mass fractionation by assuming a fixed value for a certain isotope ratio,

$$R_{ij} = r_{ij}\left(\frac{R_{kj}^{STD}}{r_{kj}^{SMP}}\right)^{\frac{\ln(m_i)-\ln(m_j)}{\ln(m_k)-\ln(m_j)}}$$

Including the epsilon notation we get the following,

$$\varepsilon R_{ij}^{SMP} = \left[\left(\frac{r_{ij}^{SMP}}{R_{ij}^{STD}}\right)\left(\frac{r_{kj}^{SMP}}{R_{kj}^{STD}}\right)^{-Q_i} - 1\right] \times 10^4$$

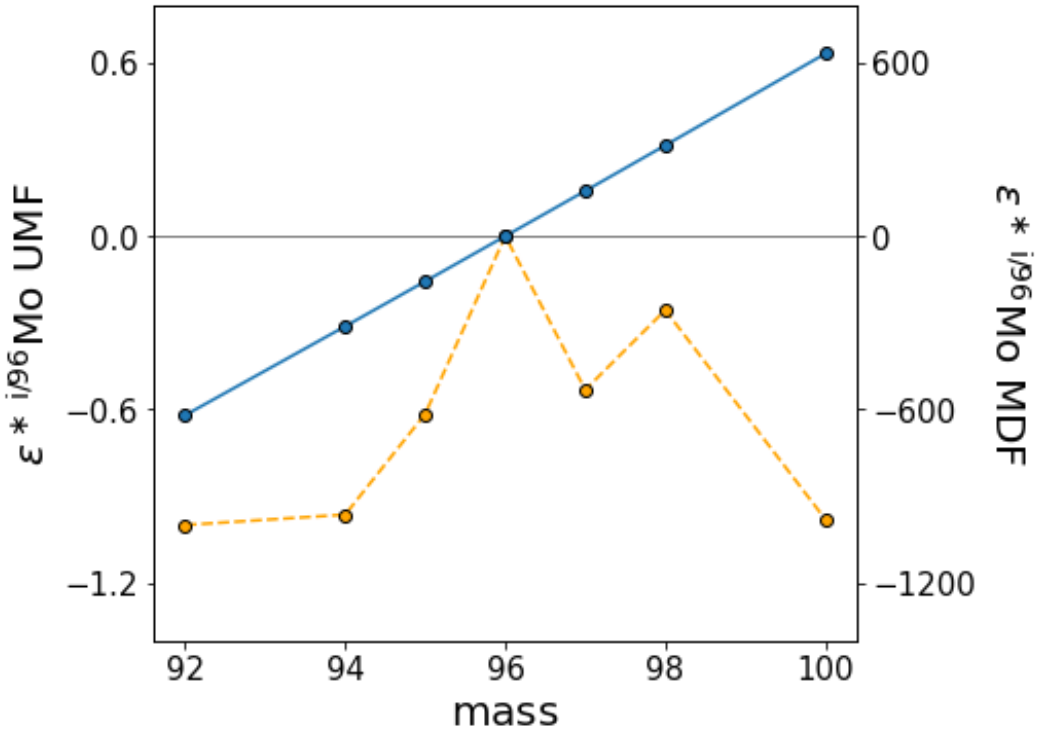

$$\varepsilon R_{ij} = \left(\frac{R_{ij}^{SMP}}{R_{ij}^{STD}} - 1\right) \times 10^4$$

Instrumental mass fractionation follows the exponential law,

$$R_{ij} = r_{ij}\left(\frac{m_i}{m_j}\right)^{-\beta}$$

Internal normalisation is correcting for mass fractionation by assuming a fixed value for a certain isotope ratio,

$$R_{ij} = r_{ij}\left(\frac{R_{kj}^{STD}}{r_{kj}^{SMP}}\right)^{\frac{\ln(m_i)-\ln(m_j)}{\ln(m_k)-\ln(m_j)}}$$

Including the epsilon notation we get the following,

$$\varepsilon R_{ij}^{SMP} = \left[\left(\frac{r_{ij}^{SMP}}{R_{ij}^{STD}}\right)\left(\frac{r_{kj}^{SMP}}{R_{kj}^{STD}}\right)^{-Q_i} - 1\right] \times 10^4$$

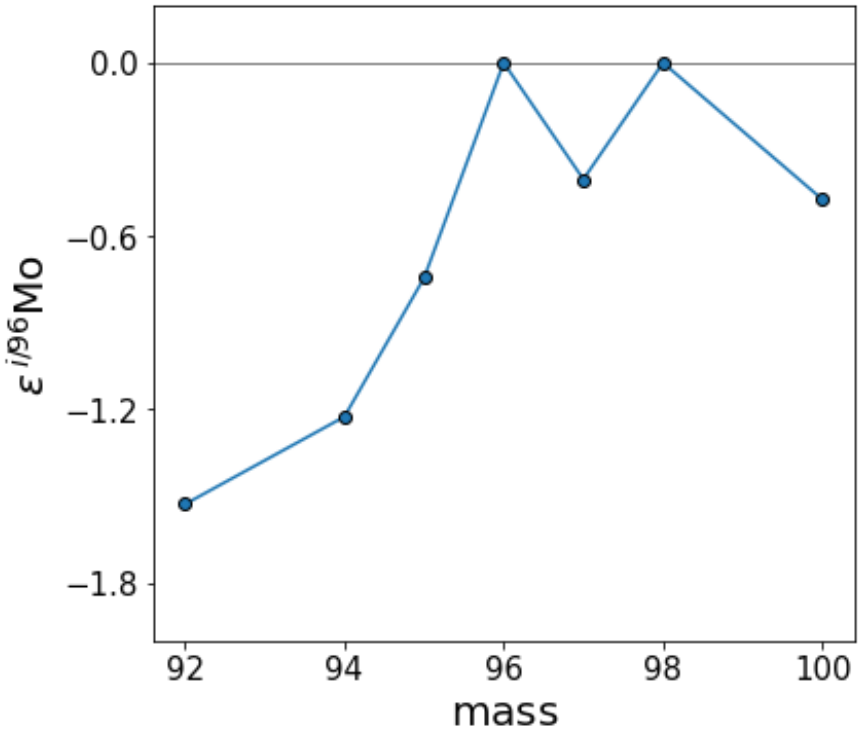

$$\varepsilon R_{ij} = \left(\frac{R_{ij}^{SMP}}{R_{ij}^{STD}} - 1\right) \times 10^4$$

Nucleosynthetic variation in bulk meteorites and CAI's exist for many **refractory** elements heavier than Fe.

More volatile elements show smaller or no nucleosynthetic variation.

The nucleosynthetic variation in bulk meteorites is often correlated between elements and consistent with an *s*-process deficit relative to Earth.

	Internal normalisation	Stardust
Element	Ratio	Isotope
Fe	57/54	56
	57/56	
Ni	61/58	58
	62/58	
	62/61	
Zn	67/64	
	68/64	
Sr	86/88	86
Zr	94/90	94
Mo	98/96	96
Ru	99/101	100
Pd	108/105	
Ba	134/136	136
	134/138	
Nd	146/144	144
Sm	147/152	149
Er	166/168	168
Yb	174/172	172
Hf	179/177	178
		180
W	186/183	184
	186/184	

Nucleosynthetic variation in bulk meteorites and CAI's exist for many **refractory** elements heavier than Fe.

More volatile elements show smaller or no nucleosynthetic variation.

The nucleosynthetic variation in bulk meteorites is often correlated between elements and consistent with an *s*-process deficit relative to Earth.

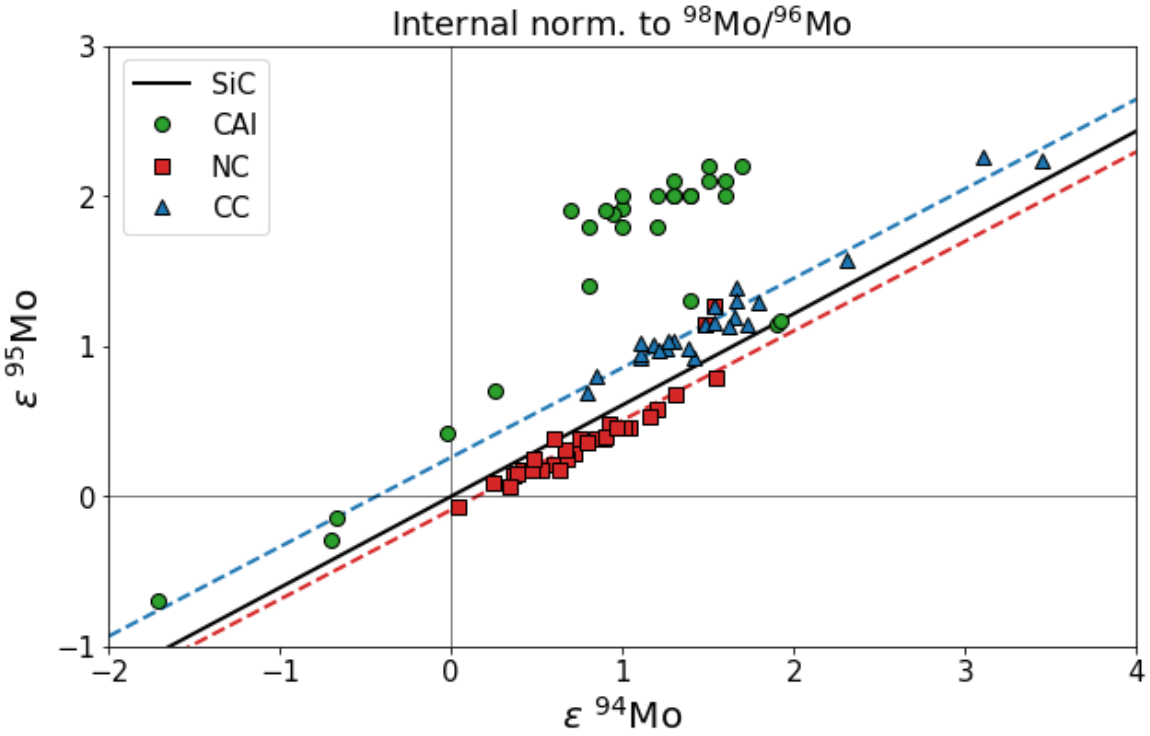

We **cannot** apply the internal normalisation equation directly on stellar yields due to the exponential nature of the equation

$$\varepsilon R_{ij}^{SMP} = \left[\left(\frac{r_{ij}^{SMP}}{R_{ij}^{STD}} \right) \left(\frac{r_{kj}^{SMP}}{R_{kj}^{STD}} \right)^{-Q_i} - 1 \right] \times 10^4$$

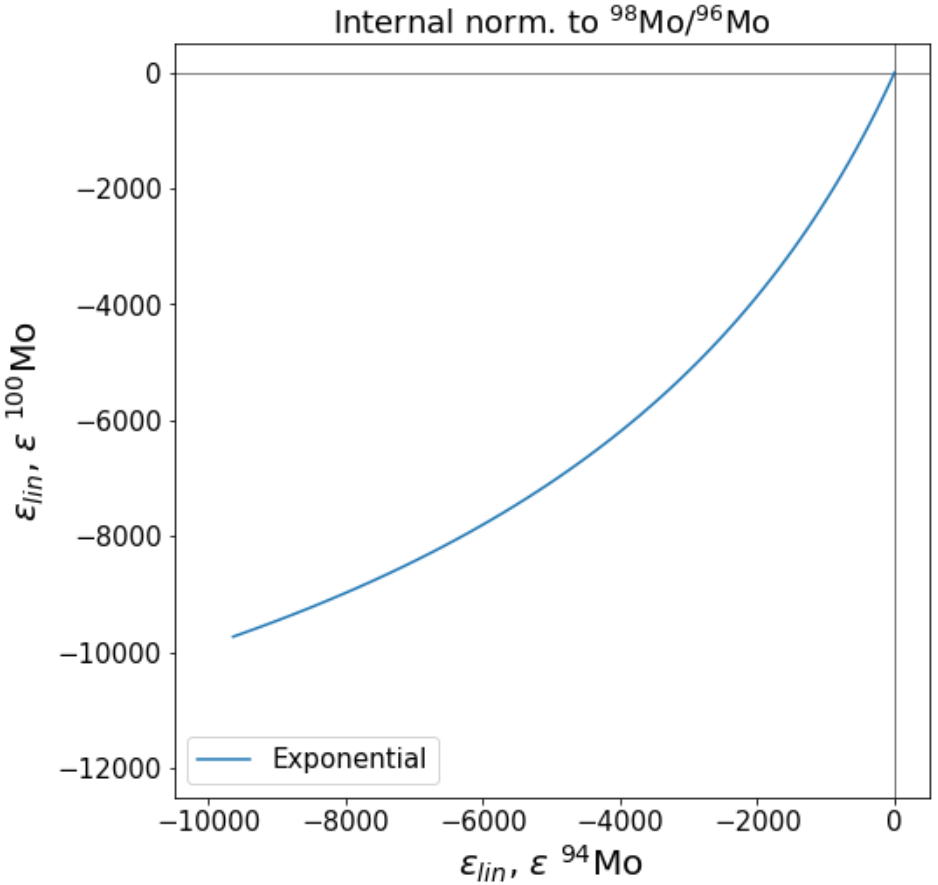

We **cannot** apply the internal normalisation equation directly on stellar yields due to the exponential nature of the equation

$$\varepsilon R_{ij}^{SMP} = \left[\left(\frac{r_{ij}^{SMP}}{R_{ij}^{STD}}\right)\left(\frac{r_{kj}^{SMP}}{R_{kj}^{STD}}\right)^{-Q_i} - 1\right] \times 10^4$$

However, we can use a linearised version of the equation for comparison with meteorite data.

$$\varepsilon R_{ij}^{SMP} \simeq \varepsilon_{lin} R_{ij}^{SMP} = \left[\left(\frac{r_{ij}^{SMP}}{R_{ij}^{STD}} - 1\right) - Q_i\left(\frac{r_{kj}^{SMP}}{R_{kj}^{STD}} - 1\right)\right] \times 10^4$$

This equation is approximately the same as that in Dauphas *et al.,* Earth Planet. Sci. Lett. **226** 2004

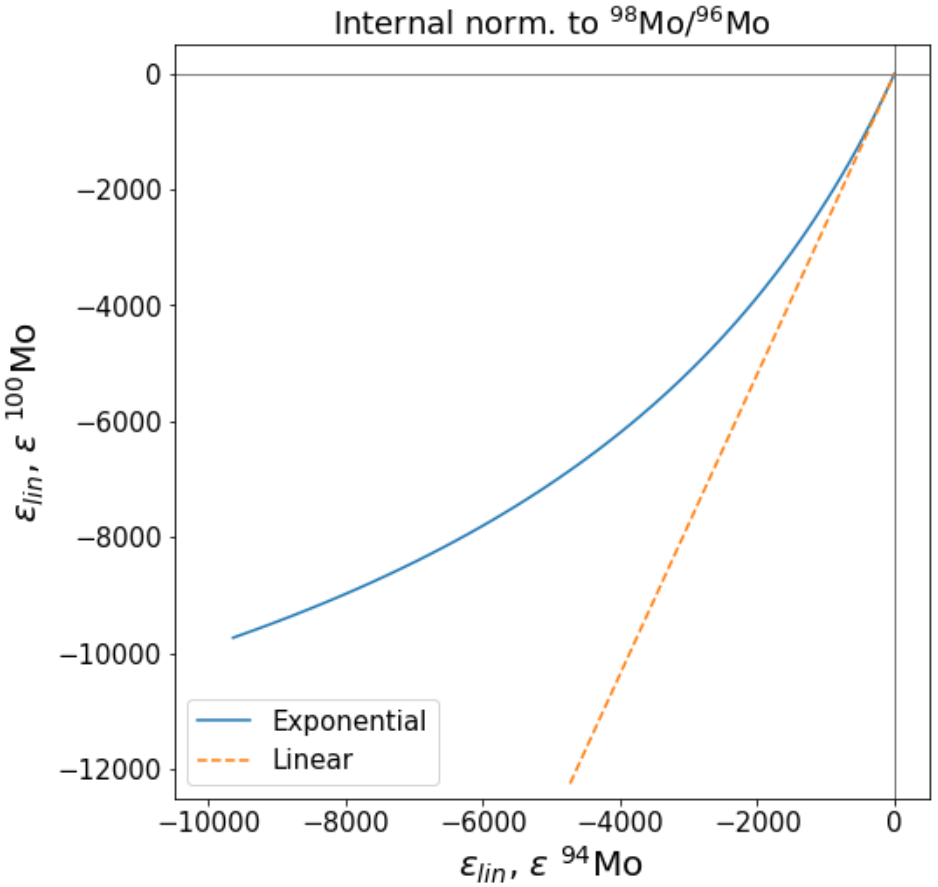

We **cannot** apply the internal normalisation equation directly on stellar yields due to the exponential nature of the equation

$$\varepsilon R_{ij}^{SMP} = \left[\left(\frac{r_{ij}^{SMP}}{R_{ij}^{STD}}\right)\left(\frac{r_{kj}^{SMP}}{R_{kj}^{STD}}\right)^{-Q_i} - 1\right] \times 10^4$$

However, we can use a linearised version of the equation for comparison with meteorite data.

$$\varepsilon R_{ij}^{SMP} \simeq \varepsilon_{lin} R_{ij}^{SMP} = \left[\left(\frac{r_{ij}^{SMP}}{R_{ij}^{STD}} - 1\right) - Q_i\left(\frac{r_{kj}^{SMP}}{R_{kj}^{STD}} - 1\right)\right] \times 10^4$$

This equation is approximately the same as that in Dauphas *et al.,* Earth Planet. Sci. Lett. **226** 2004

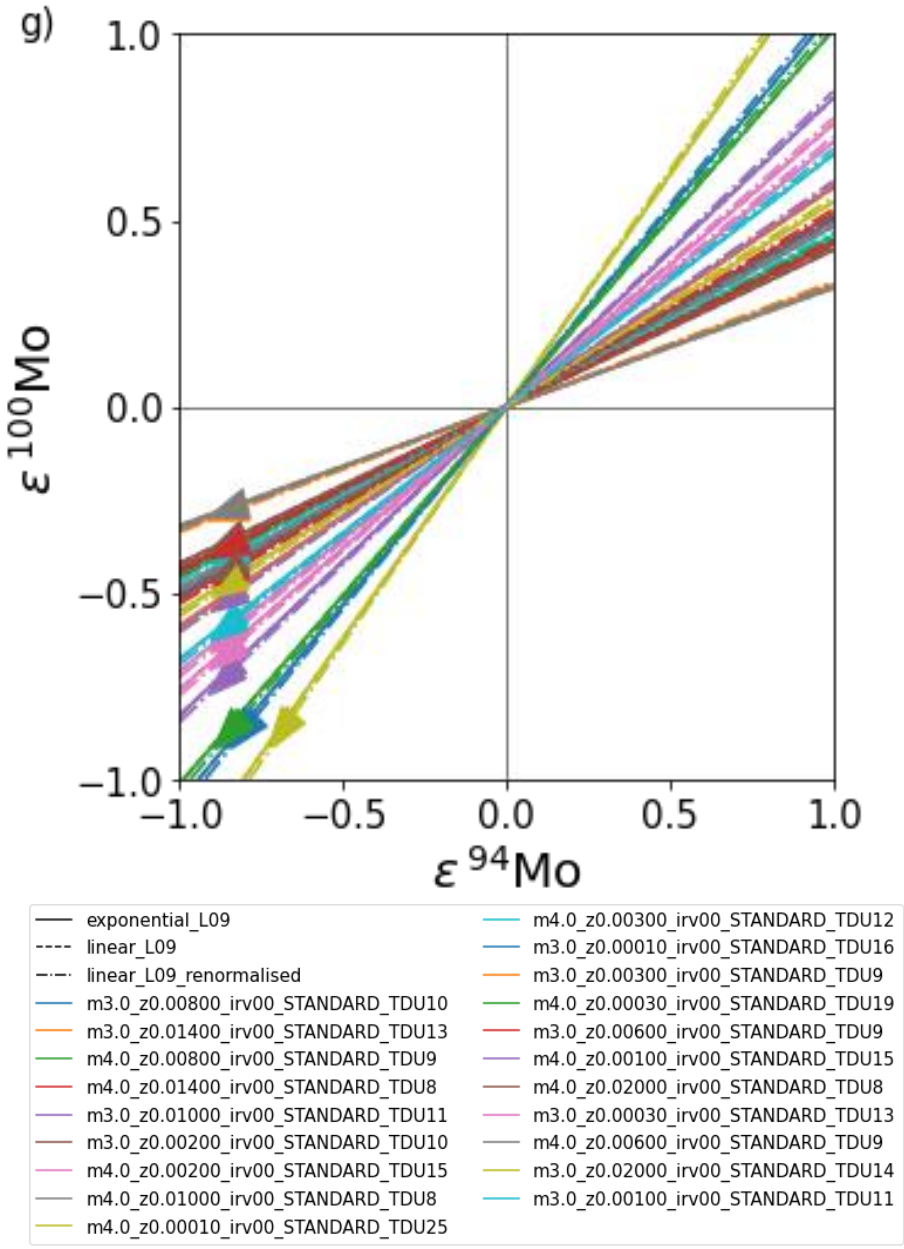

If all isotopes are readily produced by the stellar model, the choice of the STD abundances is typically negligible.

Isotopes that are not readily produced by the stellar model can be very sensitive to the STD abundance used. Even differences in the 5th decimal can result in significantly different mixing line.

We therefore suggest using the STD abundances that were used to represent the initial composition of the model.

It is also important to look at the production factors to evaluate the appropriateness of calculating mixing line.

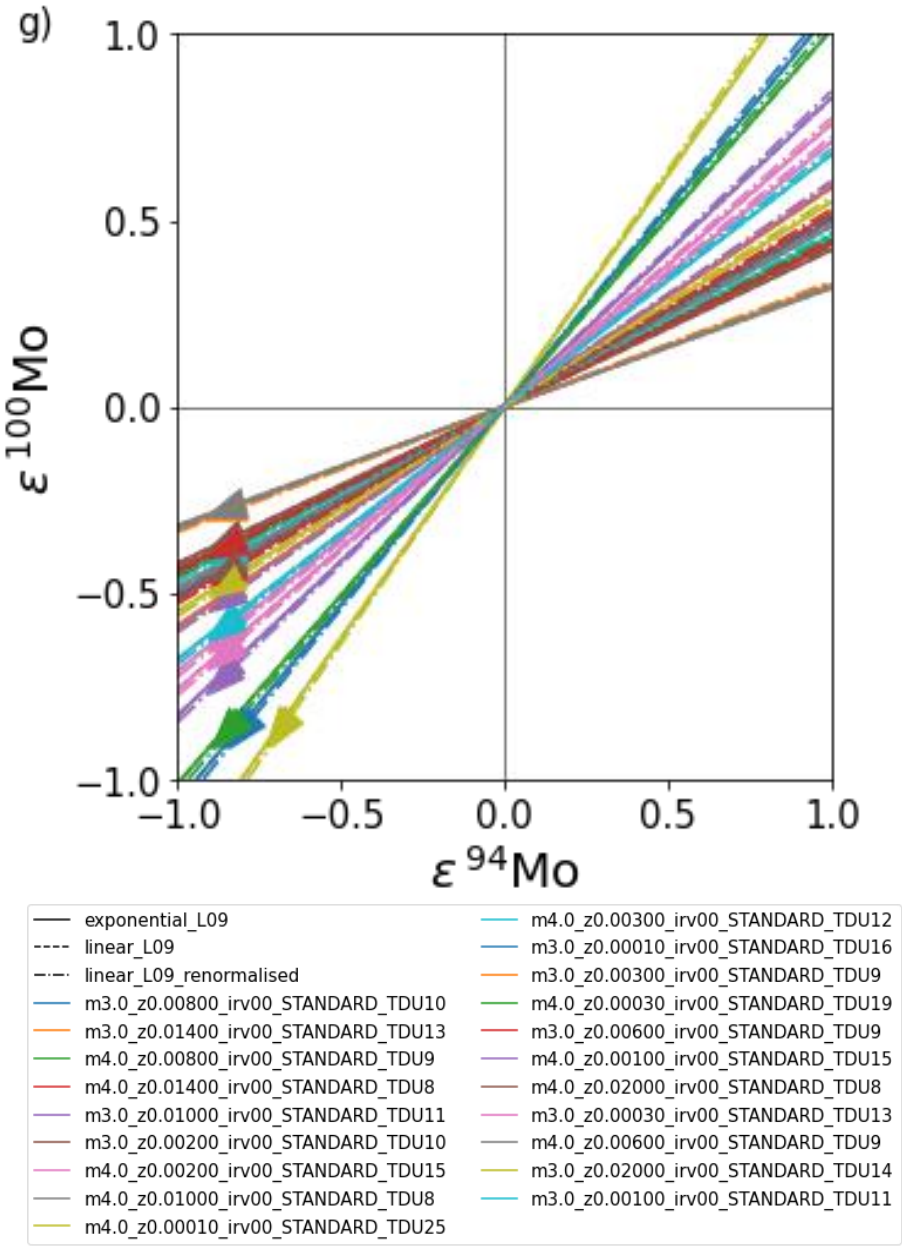

There are four Sr isotopes so therefore 12 choices for internal normalisation.

However, mixing lines will be the same for a ratio and its reverse, e.g. $^{86}Sr/^{88}Sr$ and $^{88}Sr/^{86}Sr$.

When there is a large difference in production factors between the normalising isotopes the mixing lines can change significantly.

$M = 3\ M_{\odot}$; $Z = 0.014$

Isotope	Production Factor
^{84}Sr	—
^{86}Sr	26
^{87}Sr	25
^{88}Sr	32

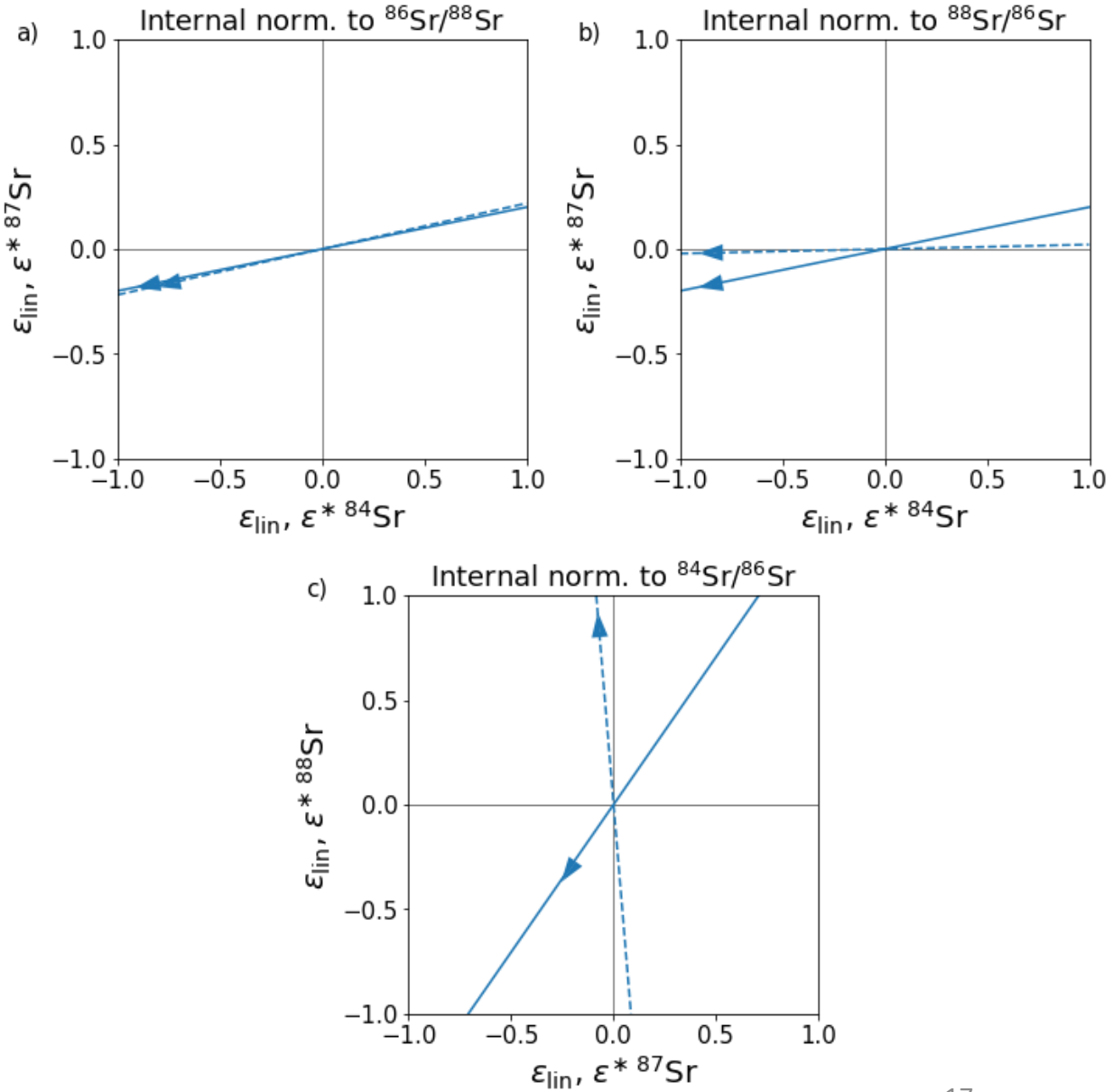

There is a small discrepancy between the *s*-process stellar models and SiC for Mo isotopes.

A higher neutron cross section has been reported for ^{95}Mo by P.E. Koehler, Phys. Rev. C **105(5)**, 2022.

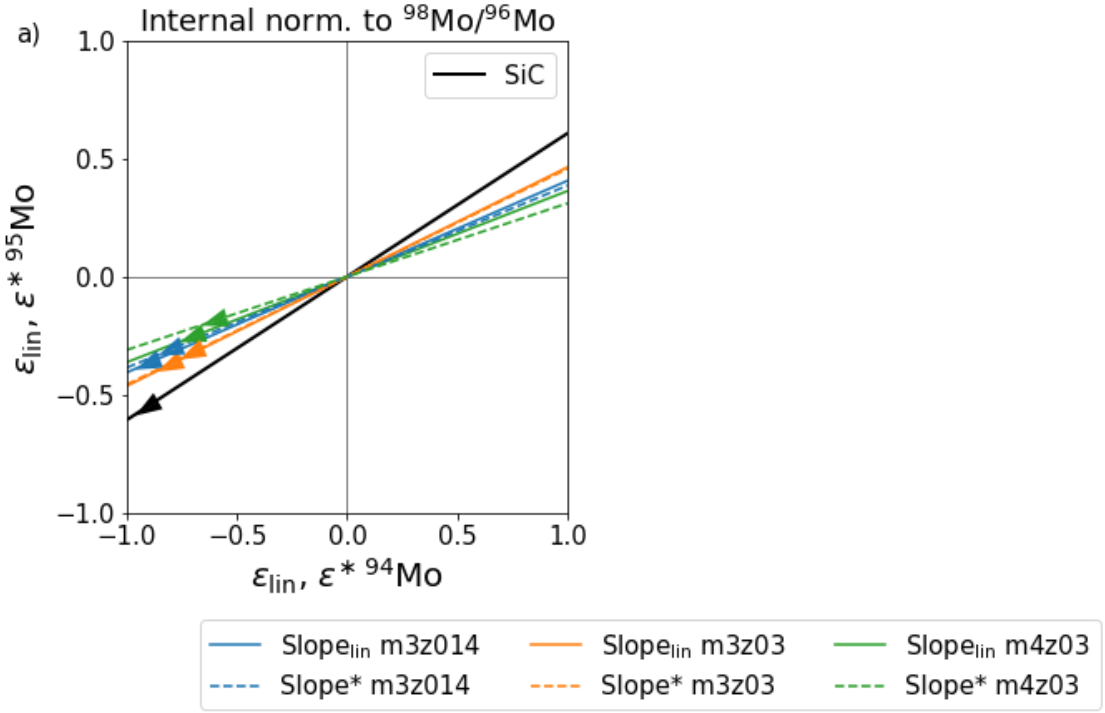

There is a small discrepancy between the *s*-process stellar models and SiC for Mo isotopes.

A higher neutron cross section has been reported for ^{95}Mo by P.E. Koehler, Phys. Rev. C **105(5)**, 2022.

The effect of the higher neutron cross section can be mimicked by dividing the abundance-by-number of ^{95}Mo by 1.3.

This updated neutron cross section results in a better agreement between stellar models and SiC for Mo isotopes.

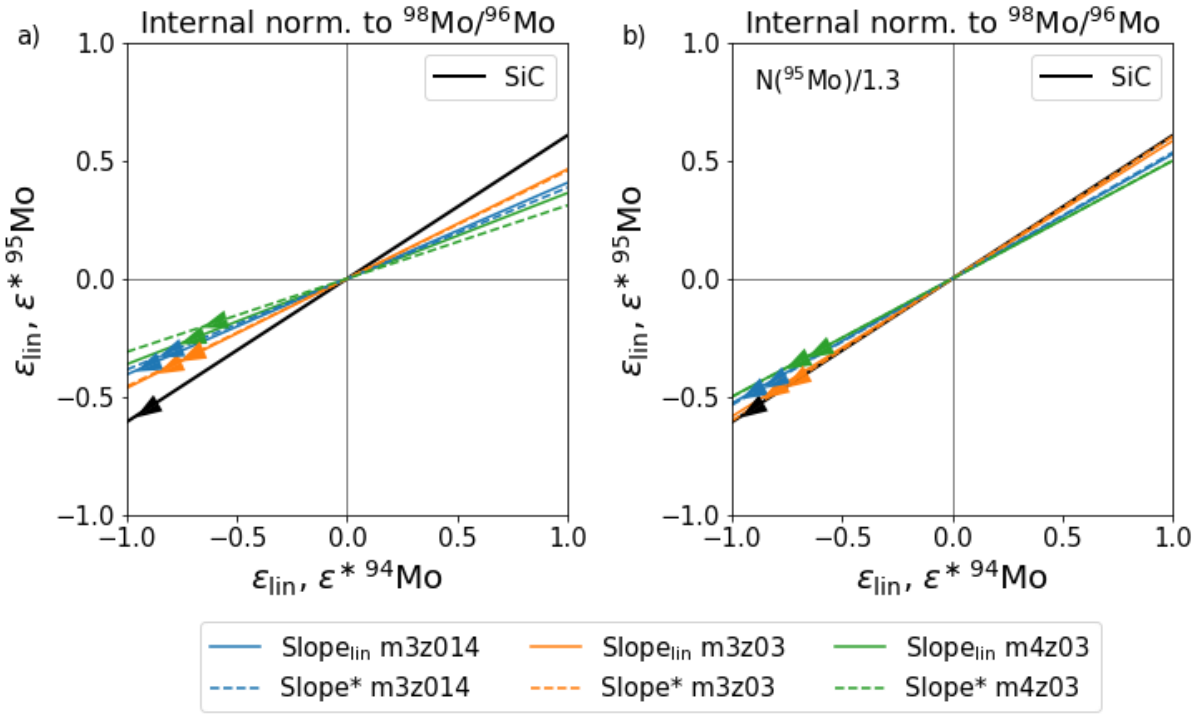

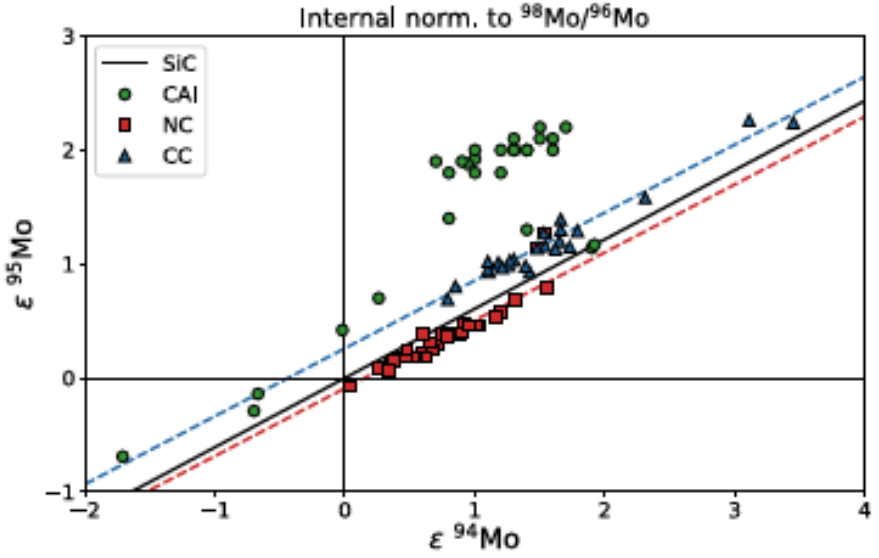

Fig. 1 Mo isotopic variations measured in different meteoritic objects, shown in the usual representation where isotopic ratios are plotted against each other. The derivation of the ϵ quantities reported on each axis is described in detail in Sect. 2.1. In brief, they are internally normalised isotopic ratios (using ^{98}Mo/^{96}Mo) relative to the laboratory standard used during the measurement (the [0,0] point by definition, close to the natural terrestrial value, but not necessarily identical). Error bars are not reported for sake of clarity, with 2σ uncertainty for most data points of the order of ± 0.1 to ± 0.5. The data are from: (i) the compilation of [39] for meteoritic bulk rocks classified in the two NC and CC groups according to their composition with respect to observed isotopic dichotomy, with the NC and CC lines from [48]; (ii) the compilation of [49] for calcium-aluminum-rich inclusions (CAIs), which have sizes of roughly a few cm, are found mostly in primitive meteorites, represent the first solids to have formed in the Solar System, and show the largest deviation from the bulk solar composition; and (iii) [50], for the the best fit trend line for meteoritic mainstream (MS) stardust silicon carbide (SiC) grains that originated from AGB stars, the main sources of the *s* process in the Galaxy

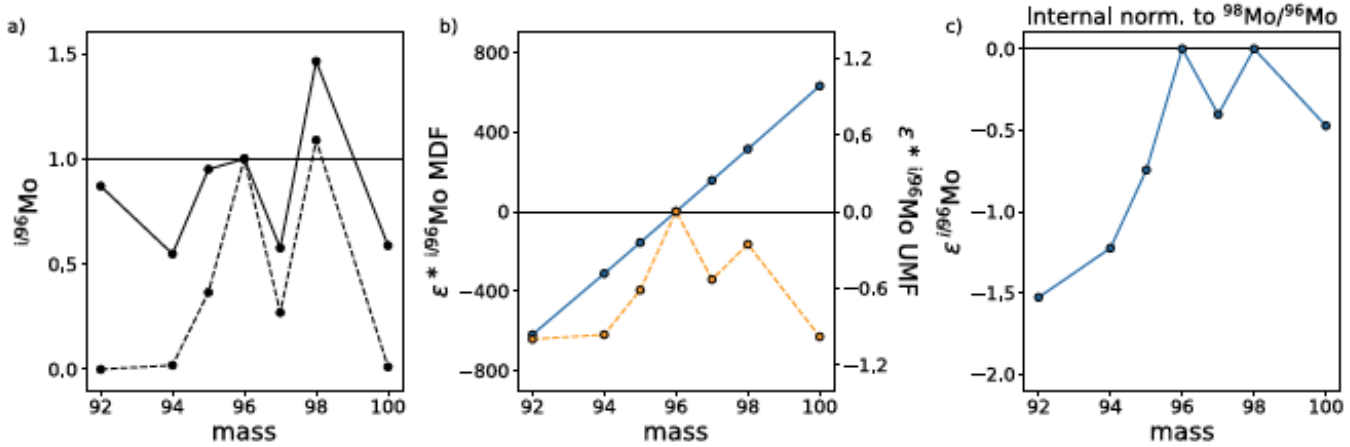

Fig. 2 Schematic description of the effect of the procedure of internal normalisation on an example *s*-process sample. In the left panel (**a**), the solid line represents the ratios of the Mo isotopes relative to ^{96}Mo using the solar abundances, the dashed line represents the same ratios calculated using the *s*-process abundances from mainstream SiC grains [50]. In the middle panel (**b**), the dashed, orange line (with corresponding values on the right y-axis) represents the ϵ values of un-mass-fractionated (UMF) *s*-process sample obtained by adding 10^{-5} of the *s*-process component to the solar abundances. The solid, blue line (with corresponding values on the left y-axis) represents the ϵ values of the sample of the dashed line, but with some added mass-dependent fractionation (MDF) obtained by adding a typical MDF effect with $\beta = 1.5$. Note the huge difference between the scale the left and right y-axes. The right panel (**c**) shows the internally normalized abundance pattern for both the MDF and UMF samples in the middle panel. Note that both lines are identical, which highlights the generality of the internal normalisation method to remove the problem of MDF

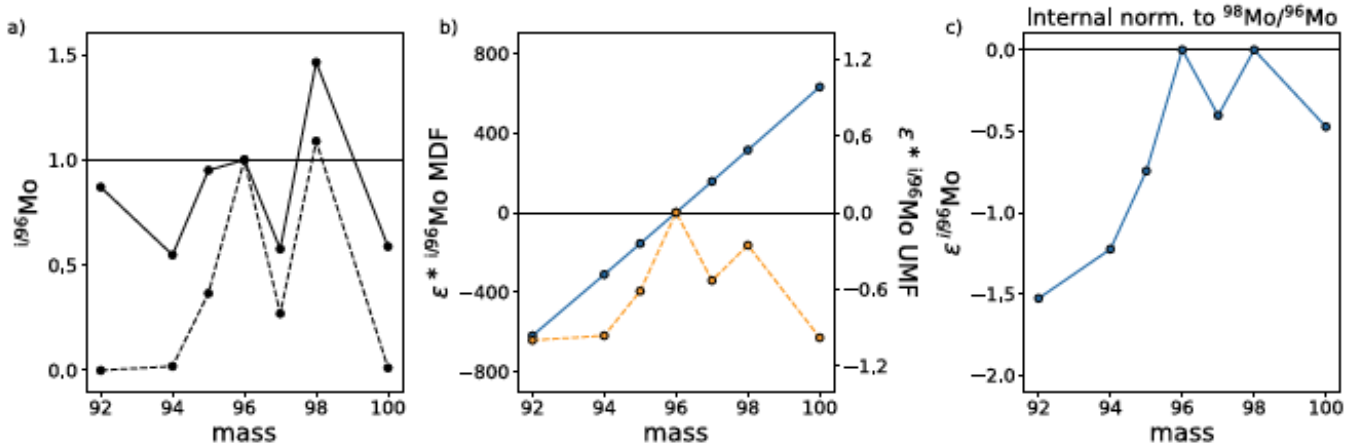

Fig. 2 Schematic description of the effect of the procedure of internal normalisation on an example *s*-process sample. In the left panel (**a**), the solid line represents the ratios of the Mo isotopes relative to ^{96}Mo using the solar abundances, the dashed line represents the same ratios calculated using the *s*-process abundances from mainstream SiC grains [50]. In the middle panel (**b**), the dashed, orange line (with corresponding values on the right y-axis) represents the ϵ values of un-mass-fractionated (UMF) *s*-process sample obtained by adding 10^{-5} of the *s*-process component to the solar abundances. The solid, blue line (with corresponding values on the left y-axis) represents the ϵ values of the sample of the dashed line, but with some added mass-dependent fractionation (MDF) obtained by adding a typical MDF effect with $\beta = 1.5$. Note the huge difference between the scale the left and right y-axes. The right panel (**c**) shows the internally normalized abundance pattern for both the MDF and UMF samples in the middle panel. Note that both lines are identical, which highlights the generality of the internal normalisation method to remove the problem of MDF

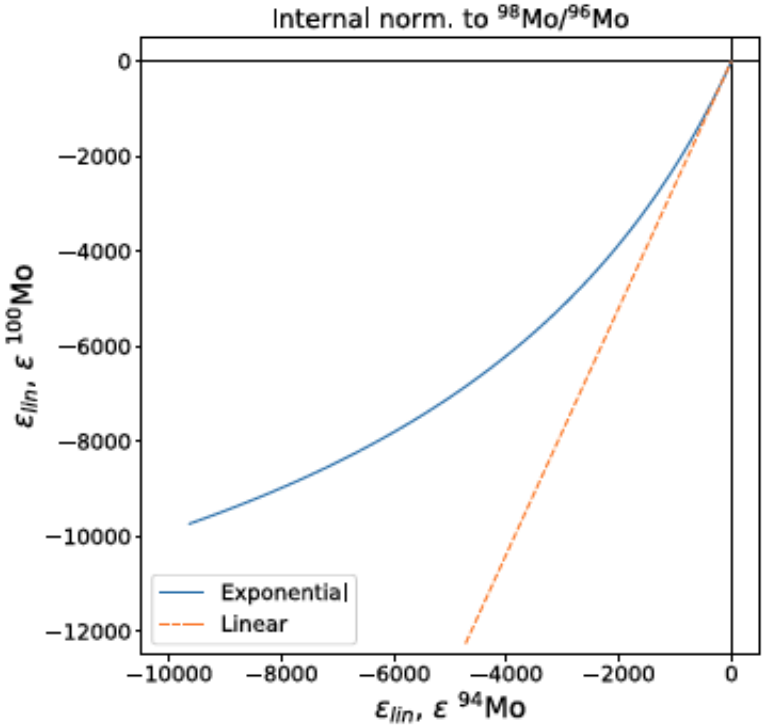

Fig. 3 Mixing lines calculated for Mo between the solar composition and the *s*-process composition, represented by mainstream SiC grains [50], using the exponential (Eq. 6; Blue solid line) and linear (Eq. 7; Orange dashed line) equations. The slopes of the two mixing lines overlap only when the offset from the solar composition (point [0, 0]) is of the order of a few 100 ϵ or less. Bulk meteorites exhibit anomalies well within this range, therefore the linear method is a valid approximation to compare the models to these data

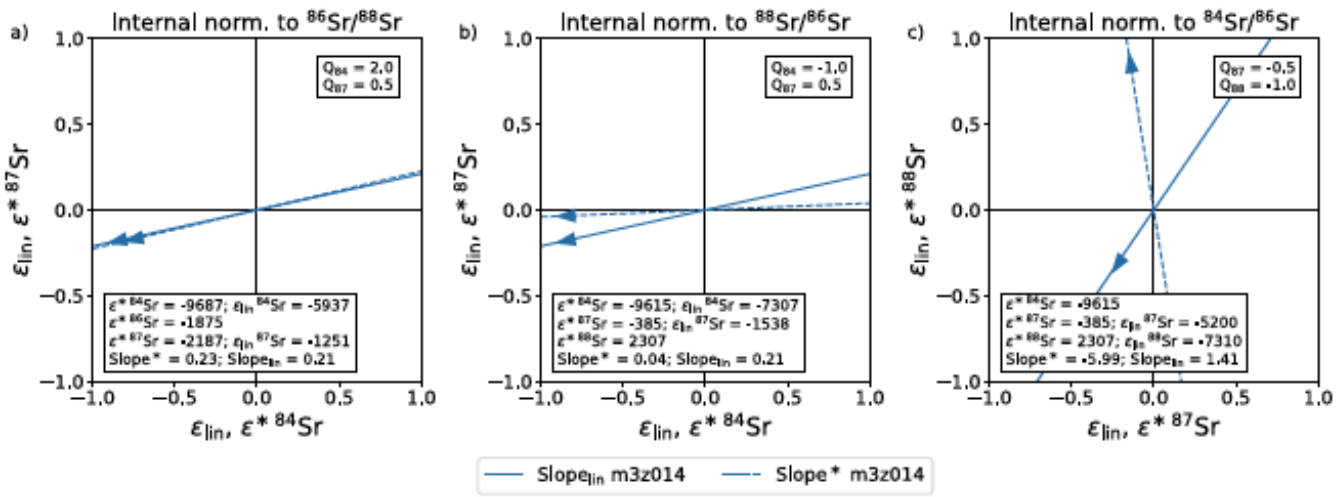

Fig. 4 Example for calculating the slope of the mixing line in the vicinity of the Solar System end-member (the [0,0] point) using the *s*-process predictions at the surface of an AGB star of initial mass 3 $M_{\odot}$ and solar metallicity (Z = 0.014) at the end of the evolution from Table 2. Solid and dashed lines represent, respectively, the slopes derived using ϵ_{lin} (i.e., the linear approximation Eq. 7) and ϵ^* (i.e., derived from applying Eq. 5 directly to the stellar abundance ratios). Here we considered 3 different possible choices of the normalising ratios, each following the top label "Internal norm. to". The arrows on each mixing line indicate the direction of the *s*-process end-member. The numerical values needed to calculate ϵ^*_{lin} are also reported, to support the clarity of the description in the text. $Slope_{lin}$ and Slope* in the legend of this figure, and following figures, refers to the slope calculated using ϵ_{lin} and ϵ^*, respectively. As the normalising ratios are indicated separately in each plot, in this and the following figures ϵ values are followed only by the isotope at numerator

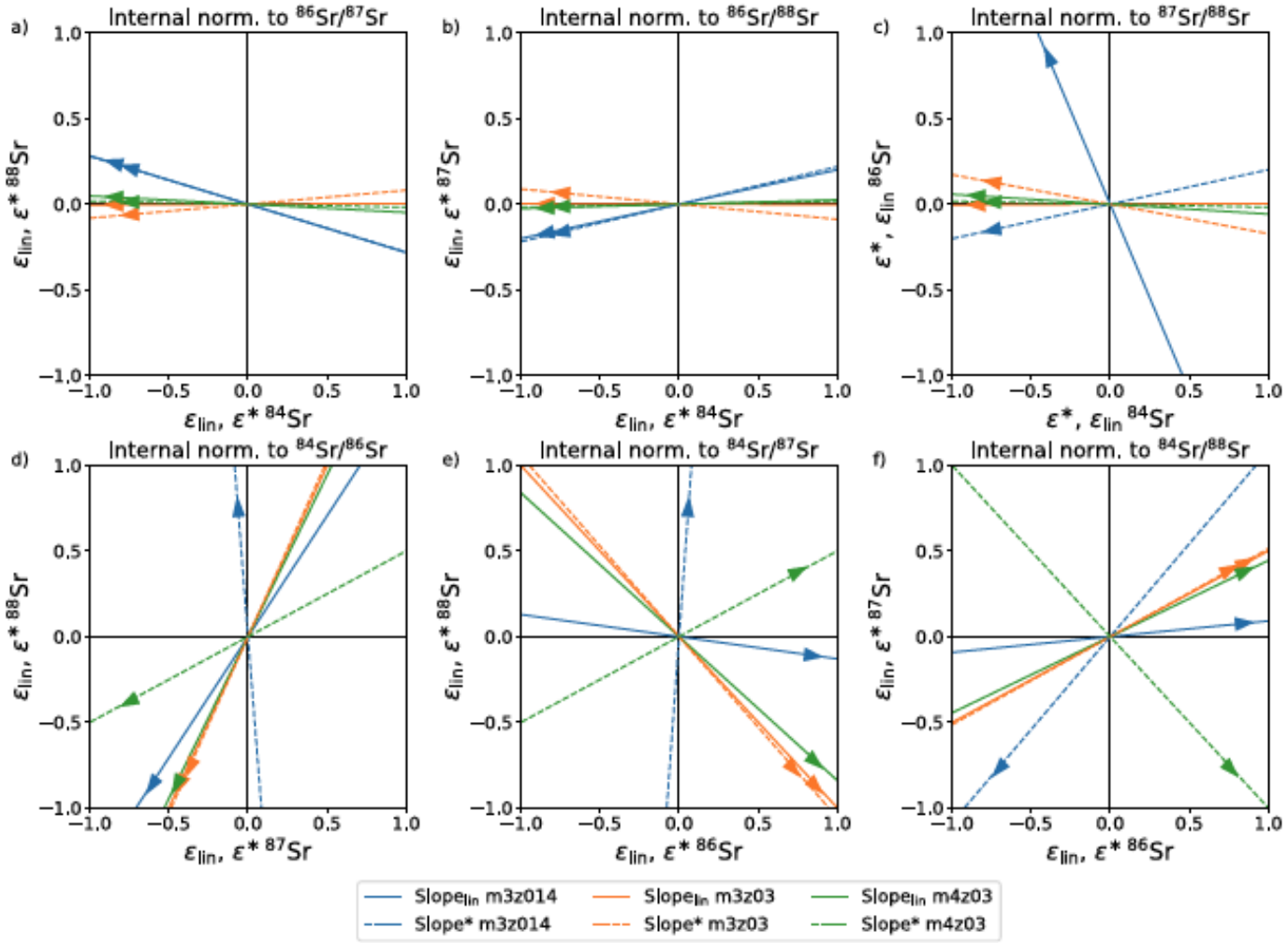

Fig. 5 Same as Fig. 4 but for the 6 possible different internal normalisation for Sr (with the corresponding internal normalisation ratio indicated at the top of each panel) applied to the three AGB models considered here ($M = 3\ M_{\odot}$ with $Z = 0.014$ and 0.03, and $M = 4$ with $Z = 0.03$), represented each with the different colors indicated in the legend

Fig. 6 Slopes predicted using the three different AGB models considered here (represented each with the color indicated in the legend) for the same Mo isotopes in the same normalisation as Fig. 1. In the right panel the abundance by number (N) of ^{95}Mo was divided by 1.3 to mimic the effect of the correspondingly higher neutron-capture cross section reported by [108]. The solid black line represents the mainstream SiC trend line from Fig. 1

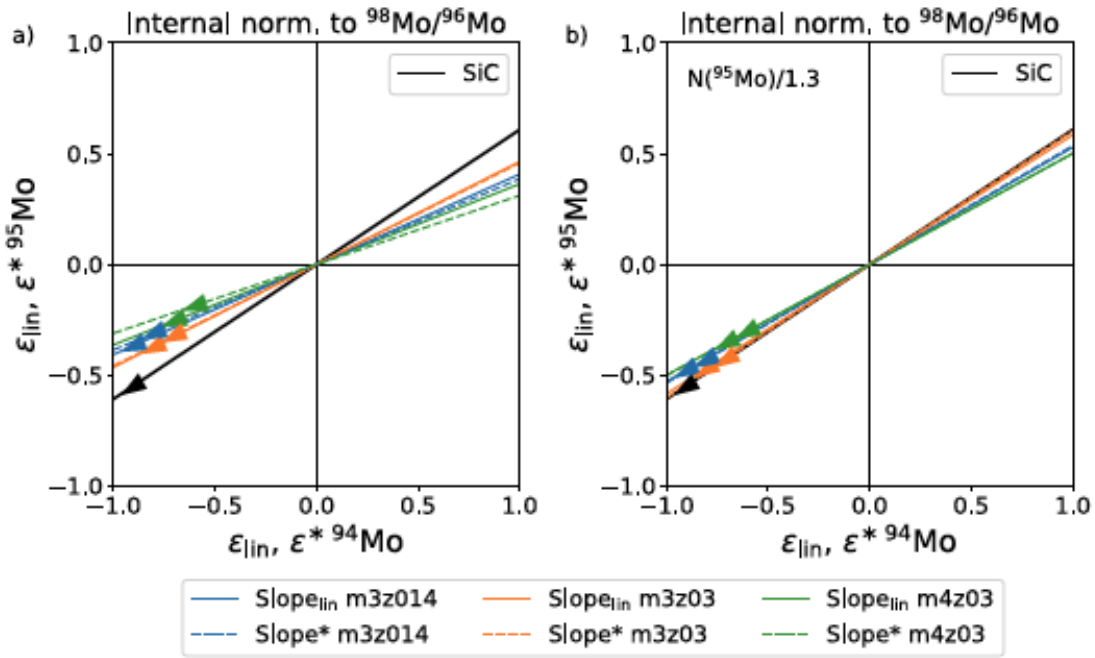

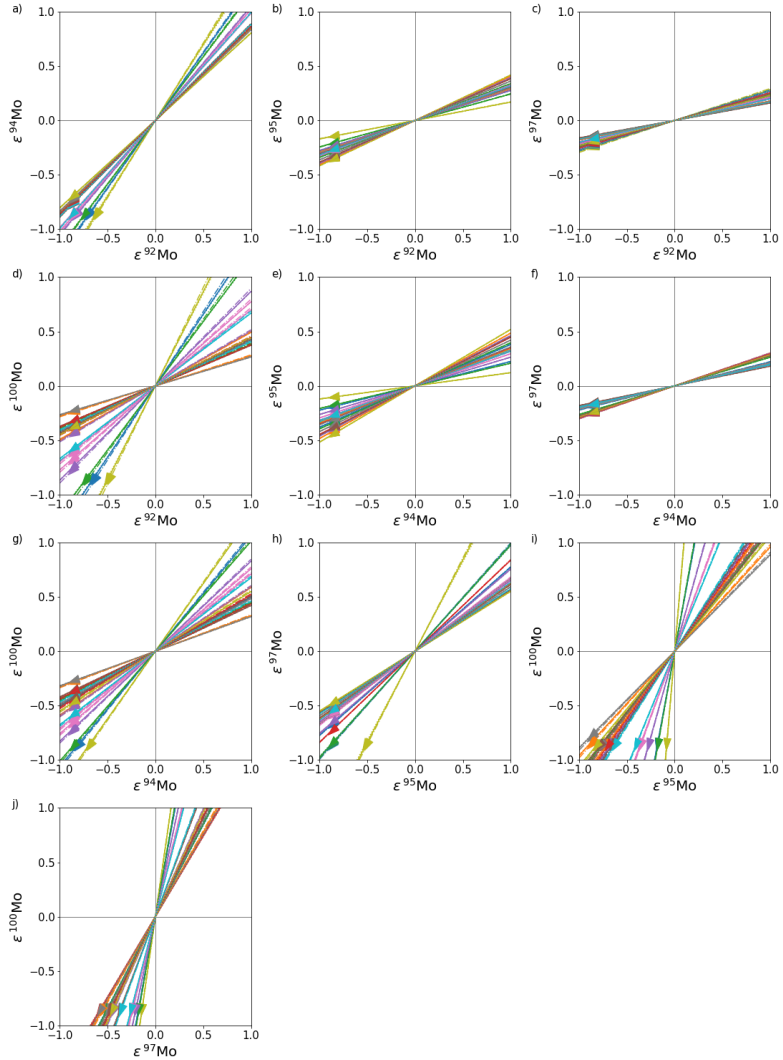
a)
b)
c)
d)
e)
f)
g)
h)
i)
j)
ε^{94}Mo
ε^{95}Mo
ε^{97}Mo
ε^{100}Mo
ε^{92}Mo
1.0
0.5
0.0
−0.5
−1.0
exponential_L09
linear_L09
linear_L09_renormalised
dauphas_L09
m3.0_z0.00800_irv00_STANDARD_TDU10
m3.0_z0.01400_irv00_STANDARD_TDU13
m4.0_z0.00800_irv00_STANDARD_TDU9
m4.0_z0.01400_irv00_STANDARD_TDU8
m3.0_z0.01000_irv00_STANDARD_TDU11
m3.0_z0.00200_irv00_STANDARD_TDU10
m4.0_z0.00200_irv00_STANDARD_TDU15
m4.0_z0.01000_irv00_STANDARD_TDU8
m4.0_z0.00010_irv00_STANDARD_TDU25
m4.0_z0.00300_irv00_STANDARD_TDU12
m3.0_z0.00010_irv00_STANDARD_TDU16
m3.0_z0.00300_irv00_STANDARD_TDU9
m4.0_z0.00030_irv00_STANDARD_TDU19
m3.0_z0.00600_irv00_STANDARD_TDU9
m4.0_z0.00100_irv00_STANDARD_TDU15
m4.0_z0.02000_irv00_STANDARD_TDU8
m3.0_z0.00030_irv00_STANDARD_TDU13
m4.0_z0.00600_irv00_STANDARD_TDU9
m3.0_z0.02000_irv00_STANDARD_TDU14
m3.0_z0.00100_irv00_STANDARD_TDU11